Segmental Motion of Supercooled Random Copolyester Studied by Neutron Polarization Analysis

Satoshi Koizumi* and Toshiya Inami

Advanced Science Research Center, Japan Atomic Energy Research Institute, Tokai-mura, Ibaraki-ken 319-1195, Japan

Received December 3, 1998; Revised Manuscript Received June 3, 1999

ABSTRACT: We investigated the segmental motion of supercooled random copolyester by elastic neutron scattering. Neutron polarization analysis was applied in order to decompose the total scattering into the coherent and incoherent contributions, which plays an essential role in the careful discussion of the scattering vector dependence of the elastic incoherent scattering. The study on highly oriented glassy random copolyester revealed the anisotropic features of segmental motions in a wide temperature region from glassy to liquid states. In this paper, we report in detail (i) the anharmonic increase of mean-square displacement, (ii) the non-Gaussian parameter $A(T)$, and (iii) the elastic incoherent structure factor for the rotational segmental motion.

I. Introduction

Neutron scattering has played an important role in the long history of glass investigation because a length scale and a time scale observed by the neutron scattering match those of the elementary class of glasses.[1] In this paper, we employ a unique combination of neutron polarization analysis[2] and an anisotropic glass of a random copolyester. The technique of neutron polarization analysis is able to decompose the total scattering into the elastic coherent and spin-incoherent contributions.[2,3] The merit of neutron polarization analysis is that the purely incoherent scattering from hydrogen can be obtained without any effort of isotope labeling. The studied random copolymer is composed of benzoic and naphthoic aromatic groups.[4] A rigid chain and a mismatch between different segmental units induce a highly oriented anisotropic glassy state. The high orientation of chains is advantageous in order to observe the aniostropic local motion of segmental units in a glassy state.

The immense interest of glass during the past 10 years has focused on so-called fragile glasses whose structural relaxation time τ_α (or viscosity) increases by many orders of magnitude in a non-Arrhenius fashion within a narrow range of temperature.[5] The non-Arrhenius behavior for fragile or intermediate systems results from the fact that the cooperativity among particles changes dramatically as the temperature decreases toward the glass transition temperature. The fragile systems below or at around T_g commonly show a fast picosecond motion which can be observed by quasi-elastic (QEL) scattering in an energy region lower than 2−3 meV.[6−11] The appearance of the fast picosecond process results in the anharmonic increase of mean-squared displacement $\langle u^2 \rangle$,[6−11] as observed by neutron scattering through Debye−Waller factor (DWF). In a kinetic scheme, the fragile glasses have been studied theoretically by a microscopic mode coupling theory (MCT), on the basis of the generalized hydrodynamics equation.[12] In this treatment, the fast picosecond motion is believed to be identical with a fast β process of MCT. Other interpretations of the fast picosecond motion have been proposed, e.g., the mode softening of vibrational density[13,14] or the short time regime of the α relaxation.[15,16] Although a concrete picture for the fast picosecond motion has not been determined yet, it is reported experimentally[6−11] that the fast picosecond motion is localized and its characteristic time is independent of both the temperature and the momentum transfer of neutrons q ($=4\pi/\lambda \sin(\theta)$), where λ and θ are a wavelength and a scattering angle, respectively. According to recent extensive investigations on glassy polymers, the onset temperature of the fast picosecond motion, which we denote by T_f, seems to be structure-independent, appearing in the temperature region from 200 to 250 K.[17] On the other hand, the calorimetric glass transition temperature T_g itself is strongly structure-dependent. Therefore, for flexible polymers, e.g., polybutadiene[8] and polychroloprene,[11] the fast picosecond motion appears from the Vogel−Fulcher temperature T_0 ($\cong T_g - 50$ K), while for polymers having more complicated structures, e.g., polystyrene[9,10] and polycarbonate,[14] it appears from far below T_g ($\sim T_g - 100$ K).

The material studied in this paper is the random copolymer of *p*-hydroxybenzoic acid (HBA) and 2-hydroxy-6-naphthoic acid (HNA) (73/27 mol/mol) (see Figure 1a). The static and dynamic properties for this material have been studied extensively by using wide-angle X-ray scattering (WAXS),[18−27] transmission electron microscopy (TEM),[28] differential scanning calorimetry (DSC),[29−31] nuclear magnetic resonance (NMR),[32,33] dielectric relaxation,[34] and dynamic mechanical analysis (DMA).[35,36] The intrachain structure is a completely random sequence of HBA and HNA.[18−22] This material exhibits a nematic order above a melting point T_m (=553 K),[23] at which there is small difference of the enthalpy or the entropy as compared with the case of normal polymers.[29] During a solidification above 500 K after quenching from above T_m, the interchain crystalline ordering takes places by slow and fast processes.[24] For example, under isothermal conditions at 505 K, the fast process proceeds within the order of a minute forming a pseudohexagonal lattice of low order, while the slow

* To whom correspondence should be addressed: TEL +81-29-282-6831, FAX +81-29-282-6716, E-mail koizumi@neutrons.tokai.jaeri.go.jp.

10.1021/ma981876h CCC: $18.00
Published on Web 07/28/1999

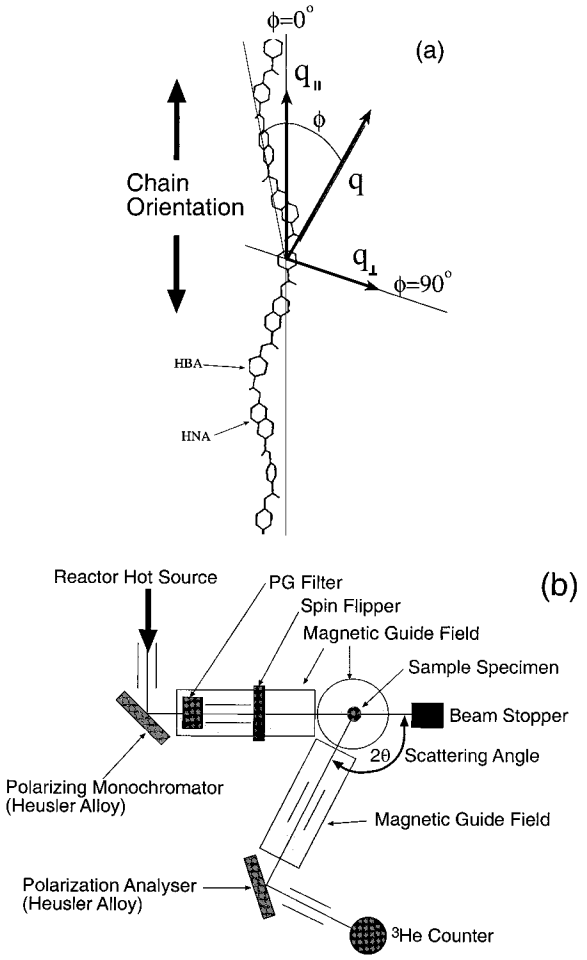

Figure 1. (a) Schematic diagram for a random copolyester composed of HBA and HNA (73/27 mol/mol). The symbols $q_{\parallel}$ and $q_{\perp}$ define scattering vectors, which are parallel ($\phi = 0°$) and perpendicular ($\phi = 90°$) to a rigid chain direction, respectively. (b) Optical setup for neutron polarization analysis. Heusler alloys are employed as a polarizing monochromator and a polarization analyzer. A magnetic guide field covers a whole scattering path from a monochromator to an analyzer. A spin flipper is placed between a monochromator and a sample position.

process proceeds on the order of 10^4 min, forming a highly ordered segmental packing in a orthorhombic lattice. The typical crystallinity of prepared films is below 15 vol %.[23] The copolymerization of two different aromatic groups is crucial to avoid the perfect crystallization due to a mismatch in a same lattice. Therefore, the glassy matrix has T_g of about 383 K.[31,36]

On the basis of these experiments, two structural models for the microcrystalline phase have been proposed.[4] Windle et al. proposed a nonperiodic layer (NPL) model,[37,38] in which rigid chains might segregate between two different monomers, moving along chain directions, and finally search identical residues (slow process). As a result of the segregation, the matching sequences along a chain form microcrystals. Blackwell et al., on the other hand, proposed the paracrystalline lattice (PCL) model,[39] which allows two different monomers to coexist in a same lattice having a conformational correlation between adjacent chains. In this model, the slow process corresponds to a conformational transition from a conformationally disordered state (CONDIS) to a more correlated state.

We investigated the segmental motions of the supercooled random copolyester by using an elastic window of neutron scattering. Neutron polarization analysis plays an essential role in the careful discussion of the non-Gaussianity of the elastic incoherent scattering and the elastic incoherent structure factor (EISF). As the temperature increases toward T_g, we observed a crossover from Gaussian to non-Gaussian q behaviors, which induces the anharmonic increase of mean-square displacement $\langle u^2 \rangle$ and the non-Gaussian parameter $A(T)$. We discuss the physical origin of non-Gaussian parameter from both static and kinetic points of view. In a nematic phase above T_m, we discuss EISF for the segmental motion, based on a Fickian free rotational model.

II. Experimental Section

1. Sample Specimens. The studied copolyester of HBA and HNA (73/27 mol/mol) is schematically described in Figure 1a. We stress that hydrogen is only on the aromatic rings in this material. The composition of 73/27 mol/mol between different-size units is crucial to achieve a glassy state as similar to a molecular dynamics (MD) simulation. The number-averaged molecular weight is about 2.0×10^4. We prepared the oriented film specimens by extrusion from melts. For scattering measurements, we annealed them above T_m and quenched in water. The preferential orientation in a nematic phase remains during a solidification below T_m to form an anisotropic glassy state ($T_g = 383$ K).[40] We performed the scattering measurements under isothermal conditions by successively increasing the temperature from room temperature. Therefore, we can believe that the static structure of specimens was stable during our measurements at least up to 500 K, where the slow ordering process starts to proceed.[24]

2. Optical Setup for Neutron Polarization Analysis. We performed neutron polarization analysis on the polarization triple axis spectrometer TAS-1 at JRR3M at Japan Atomic Energy Research Institute (JAERI) in Tokai. Figure 1b shows our optical setup schematically. We employed Heusler alloys (Cu_2MnAl)[3] as a polarizing monochromator and a polarization analyzer. The second Heusler alloy analyzes a spin state and an energy transfer of scattered neutrons simultaneously. A magnetic guide field, which defines a direction of polarization, covers a whole path from the polarizing manochromator to the polarization analyzer. We allocate both the polarizing manochromator and the polarization analyzer to reflect neutrons of a same spin state (for example, up (+)) toward a direction of the scattering path. A spin flipper is placed between the polarizer and the sample position. We used an incident neutron wavelength of $\lambda = 2.43$ Å, producing an energy resolution of $\Delta E = 0.8$ meV at the elastic position and a polarization of 90 ± 1%. Parts of the scattering measurements were performed using unpolarized neutrons. In this case, we employed a pyrolytic graphite (PG (002)) as a monochromator and an analyzer on the same spectrometer of TAS-1. Because of the comparable mosaic spread, we obtained similar energy resolutions for both polarized and unpolarized neutrons. We choose the scattering vector $\tilde{q}$ to be either parallel ($q_{\parallel}$, $\phi = 0°$) or perpendicular ($q_{\perp}$, $\phi = 90°$) to the orientational direction, where ϕ is an angle between the rotational axis and $\tilde{q}$ (see Figure 1a). The obtained spectra were corrected for absorption and background scattering. We neglected the multiple scattering effect in our data analyses because the transmission was more than 90%.

III. Scattering Law and Theoretical Details

1. Neutron Polarization Analysis. We summarize neutron polarization analysis, which we employ in order to decompose the total scattering into the coherent and incoherent contributions. More detailed descriptions are in refs 2, 3, and 41. The magnetic guide field defines a direction of polarization (up (+) or down (−)). As mentioned above, we allocate the polarizing manochro-

mator and the polarization analyzer to reflect only the (+) neutrons toward the scattering path. The spin flipper, allocated between the polarizing manochromator and the sample position, can change the spin state of incident neutrons. With the spin flipper *on*, the (−) neutron passes through the sample position, while with the spin flipper *off*, the (+) neutron passes. A spin state of neutrons is influenced by the scattering process in a sample, whether coherent or incoherent scattering. Finally the second crystal of polarization analyzer can reflect only the (+) neutron toward a counter. Therefore, in the case of the spin flipper *on*, we observe the spin flip scattering process (−,+), while in the case of the spin flipper *off*, we observe the spin nonflip scattering process (+,+).

The differential scattering cross sections for the (−,+) or (+,+) scattering process can be given as follows:[3]

$$\left(\frac{d\sigma}{d\Omega}\right)_{(-,+)} \sim \frac{2}{3}\left(\frac{d\sigma}{d\Omega}\right)_{INC}$$

$$\left(\frac{d\sigma}{d\Omega}\right)_{(+,+)} \sim \frac{1}{3}\left(\frac{d\sigma}{d\Omega}\right)_{INC} + \left(\frac{d\sigma}{d\Omega}\right)_{COH} \quad (1)$$

where the abbreviations of INC and COH denote incoherent and coherent, respectively. The (−,+) scattering process is composed of the incoherent scattering, while the (+,+) scattering process is composed of both the coherent and incoherent scattering. If we observe a set of the (−,+) and (+,+) scattering cross sections by operating the spin flipper *on* and *off*, we can obtain the coherent and incoherent contributions according to eq 1.

2. Elastic Incoherent Scattering Law. The total neutron scattering is composed of both the coherent and incoherent scattering.

$$S_{total}(q,\omega) \sim S_{coh}(q,\omega) + S_{inc}(q,\omega) \quad (2)$$

The incoherent scattering has information on the self-correlation of nucleus's motion, while the coherent scattering has information on the pair correlation. In general, hydrogenated specimens, e.g., organic material, are characteristic of having the strong incoherent scattering of hydrogen as compared with the coherent scattering of other atoms. However, if we observe a highly oriented system, for example, we have an intense coherent contribution at a certain scattering angle. For a selective observation of the coherent or incoherent scattering, it becomes a crucial problem to separate the coherent and incoherent scattering.

Let us discuss the elastic incoherent scattering law for a system where the vibrational and relaxational motions coexist. If we can neglect the coupling between the vibrational and relaxational motions, the elastic incoherent scattering function $S_{inc}(q,\omega=0)$ can be given as follows:[42]

$$S_{inc}(q,\omega=0) \sim DWF(q)[EISF(q) + \varphi QEL(q,\omega)\,\delta(\omega)] \quad (3)$$

where φ is constant. The temperature dependence of $S_{inc}(q,\omega=0)$ results from both the vibrational contribution of DWF and the relaxational contribution of EISF and QEL. Especially if the temperature is low enough to freeze the relaxational motion, $S_{inc}(q,\omega=0)$ is composed of only the vibrational contribution of DWF. EISF, in other words, a long time-averaged self-correlation of hydrogen motion, is determined by size and symmetry of a confinement space (or a cage) for the hydrogen's motion.[42]

A general form of DWF is obtained from the cumulant expansion[43]

$$DWF \sim \exp[-\langle u^2\rangle q^2 + \alpha(q)] \quad (4)$$

where $\alpha(q)$ is a non-Gaussian contribution. The Gaussian description of the first term in eq 4 is valid for ideal systems, e.g., the harmonic oscillator and the perfect gas. The non-Gaussian term $\alpha(q)$ is described by a so-called non-Gaussian parameter $A(T)$.[44] If we consider the non-Gaussian contribution up to the order of q^4, $\alpha(q)$ is given as follows:

$$\alpha(q) = {}^1/_2 A(T)[\langle u^2\rangle]^2 q^4 \quad (5)$$

A concrete form of EISF and QEL depends on a type of relaxation. Let us consider a free rotational motion, in which a nucleus (or hydrogen) can move on a circle of radius r obeying a Fickian diffusion process. This model gives EISF and QEL with the Bessel function of the first kind $J_m(x)$ as follows:[42,45]

$$EISF(q,\phi) \sim J_0^2(qr\sin\phi) \quad (6)$$

$$QEL(q,\omega,\phi) \sim 2\sum_{m=1}^{\infty} J_m^2(qr\sin\phi)\frac{1}{\pi}\frac{D_r m^2}{(D_r m^2)^2 + \omega^2} \quad (7)$$

where D_r is a rotational diffusion coefficient.

The elastic incoherent scattering function $S_{obs}(q,\omega=0)$, observed experimentally, is influenced by an instrumental resolution function $R(\omega)$. $S_{obs}(q,\omega=0)$ has a convoluted form by $R(\omega)$ with a full width at half-height ΔE as follows:

$$S_{obs}(q,\omega=0) \sim \int_{-\infty}^{\infty} S_{INC}(q,\omega')\,R(\omega)\,d\omega'|_{\omega=0} \quad (8)$$

Thus, the elastic incoherent scattering, obtained experimentally, e.g., EISF, provides us the time-averaged self-correlation up to the time of an elastic resolution limit ($\sim h/\Delta E$), where h is the Planck's constant. In other words, we observe a snapshot picture of the self-correlation taken with a shutter speed of $h/\Delta E$. For the extreme case where ΔE is infinite, the incoherent scattering is integrated over a whole energy space, as follows:

$$S_{obs}(q) \sim \int_{-\infty}^{\infty} S_{INC}(q,\omega')\,d\omega' = \text{const} \quad (9)$$

This corresponds to a pure snapshot. In this case, the incoherent scattering becomes q-independent.

IV. Experimental Results

1. Elastic Scattering with Unpolarized Neutron. Figure 2a shows the elastic scattering profiles $S(q,\omega=0)$ for $q_\perp$ obtained above 291 K. In these measurements, we employed the pyrotic graphite PG (002) as a monochromator and an energy analyzer. The unpolarized incident neutron of $\lambda = 2.43$ Å gives the elastic energy resolution of $\Delta E = 0.8$ meV at the elastic position. $S(q,\omega=0)$ is composed of the elastic coherent and elastic incoherent scattering. Below T_m (=553 K), the elastic coherent scattering exhibits a single intense maximum

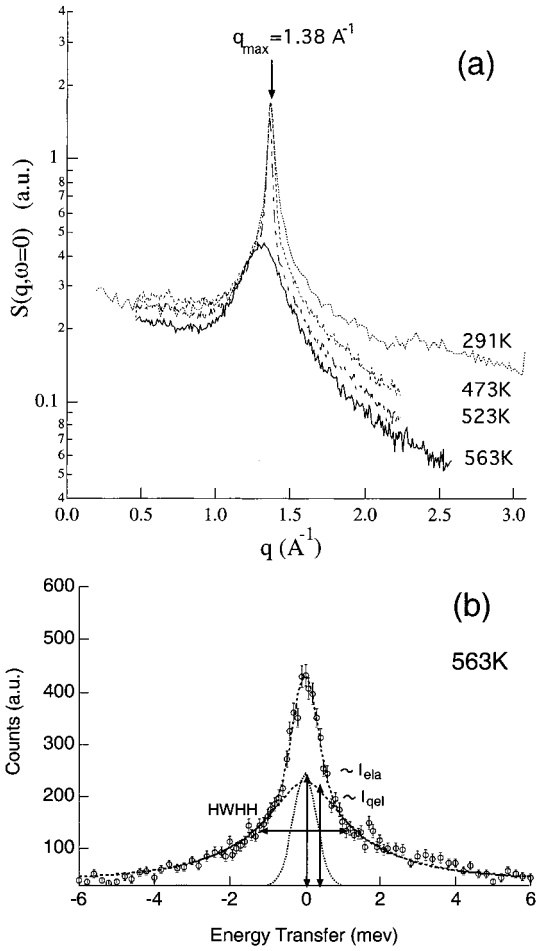

Figure 2. (a) Elastic scattering profiles $S(q,\omega=0)$ for $q_\perp$ obtained at 291, 473, 523, and 563 K with unpolarized neutrons of $\lambda = 2.43$ Å. (b) The constant q-scan profile for $q_\perp = 2.48$ Å^{-1} obtained at 563 K, which is decomposed into elastic and quasi-elastic contributions.

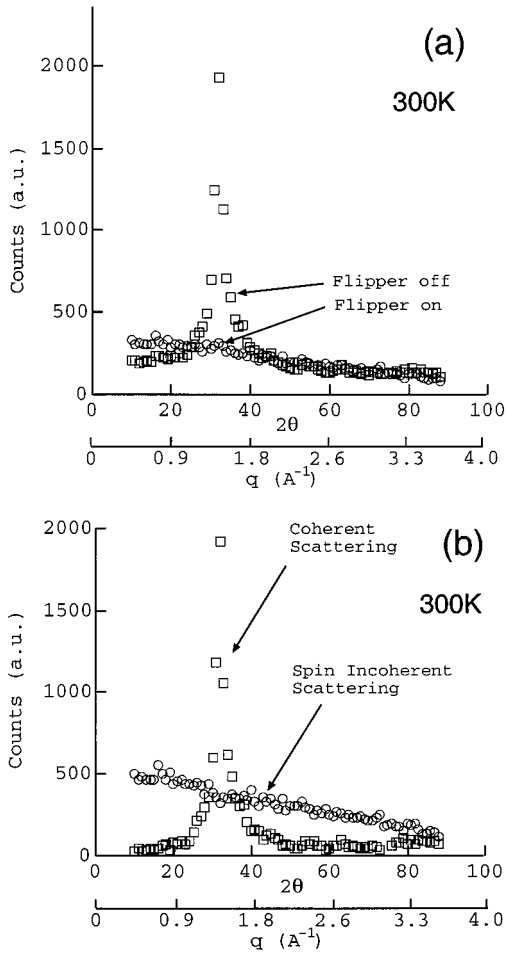

Figure 3. Demonstration of neutron polarization analysis. (a) The spin flip (−,+) and spin nonflip (+,+) scattering processes for $q_\perp$ obtained at 300 K. (b) Elastic coherent and incoherent scattering for $q_\perp$ at 300 K, decomposed by neutron polarization analysis.

at $q = 1.38$ Å^{-1}, which originates from the interchain interference. Above T_m, it changes dramatically into a broad maximum, which is characteristic for a nematic order.[46] The elastic incoherent scattering, on the other hand, is distributed over a wide q region. As the temperature increases, the asymptotic q-behavior of the incoherent scattering becomes steeper, which is attributed to DWF or QEL.

As a counterpart of these elastic scattering, there exists the intense QEL scattering in the low-energy region. Figure 2b shows the constant q-scan profile for $q_\perp = 2.48$ Å^{-1} at 563 K. By taking into account the energy resolution, the constant q-scan profile is decomposed into the elastic and QEL components, where I_{el} and I_{qel} will denote their normalized heights. For the QEL spectra, we employed a single Lorentzian function to estimate the apparent half-width at half-height (hwhh). The q dependence of hwhh has been discussed in ref 46, on the basis of the free rotational motion for aromatic rings. The q dependence of I_{el} and I_{qel} will be discussed in sectionV.3 based on the same method.

2. Decomposition into Coherent and Incoherent Scattering by Neutron Polarization Analysis. In Figure 3, we demonstrate how successfully neutron polarization analysis decomposes the total scattering into the coherent and incoherent scattering. Figure 3a shows the elastic scattering profiles for $q_\perp$ obtained at 300 K by operating the spin-flipper *on* and *off*. As described in section III, for the case of spin-flipper *on*, we observe the (−,+) scattering process, which is composed of the incoherent scattering. On the other hand, for the case of spin-flipper *off*, we observe the (+,+) scattering process, which is composed of both the coherent and incoherent scattering. Taking into account the instrumental efficiency of polarization (=90%), the elastic coherent and incoherent scattering were successfully decomposed as shown in Figure 3b.

We observed the temperature dependence of the elastic coherent and incoherent scattering, thus decomposed by neutron polarization analysis. Parts a and b of Figure 4 show the elastic incoherent scattering profiles obtained for $q_\perp$ and $q_{||}$, respectively. As the temperature increases, the asymptotic q-behavior of the incoherent scattering becomes steeper, which is attributed to the increase of $\langle u^2 \rangle$ through DWF. In Figure 4a for $q_\perp$, the elastic incoherent profiles obtained at 453 and 573 K become non-Gaussian, deviating from a exponential decay with q^2 in a higher q-region of $q^2 > 6$ Å^{-2}. To the contrary, at 300 K we observed the exponential decay in a whole q-region. Furthermore, the elastic incoherent profile obtained at 573 K is characteristic of having a broad maximum at around $q^2 = 11$ Å^{-2}, as indicated by a thick arrow in Figure 4a. We stress that the elastic incoherent scattering for $q_{||}$ decreases exponentially with q^2 in a whole q-region and for all temperatures from 300 to 453 K (see Figure 4b).

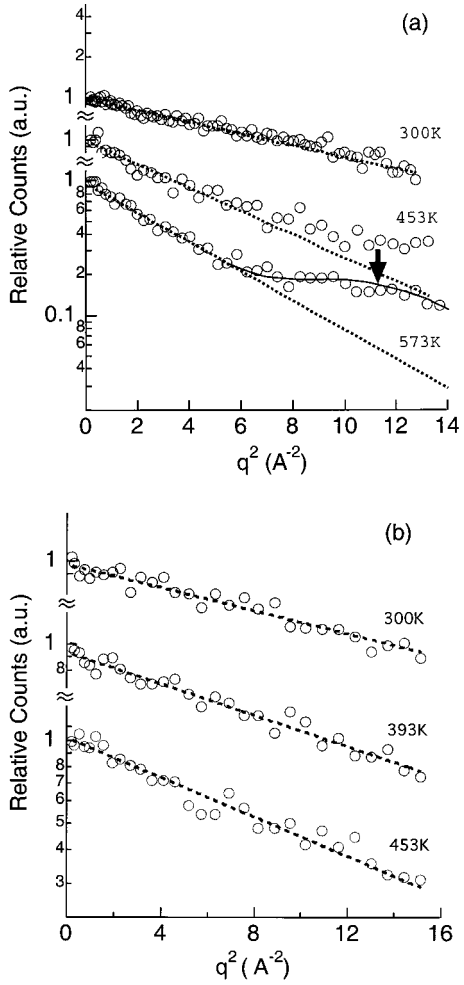

Figure 4. (a) Elastic incoherent scattering profiles for $q_\perp$ obtained at 300, 453, and 573 K. As temperature increases, asymptotic q-behaviors become non-Gaussian (at 453 and 573 K). Especially at 573 K, a broad maximum appears at around $q^2 = 11$ Å^2 as indicated by thick arrow. (b) Elastic incoherent scattering profiles for $q_{||}$ obtained at 300, 393, and 453 K, which exhibit Gaussian q-behaviors.

Thus, the anisotropic non-Gaussianity in q-behavior was visualized by the elastic incoherent scattering measurements. It is natural to suppose that this anisotroic non-Gaussianity would relate to a chemical structure, i.e., the torsional or rotational degree of freedom of aromatic rings about a chain direction.

Figure 5 shows the temperature dependence of the elastic coherent scattering profiles, decomposed by neutron polarization analysis. The elastic coherent scattering profiles below 453 K exhibit a single intense maximum at $q = 1.38$ Å^{-1}, which is identical with (110) reflection of the pseudohexagonal phase, as reported by WAXS.[23−27] In the temperature region below 453 K, its intensity and q-position (=1.38 Å^{-1}) do not change. Thus, we confirm that the interchain order does not change during our measurements up to 453 K and maintains the glassy state. At 573 K, on the other hand, the intense scattering maximum at $q = 1.38$ Å^{-1} becomes broader, reflecting a nematic order.[46]

3. Estimation of Mean-Square Displacement and Non-Gaussian Parameter. From the asymptotic q-behaviors of the elastic incoherent scattering, we estimate $\langle u^2 \rangle$ and $A(T)$ in the wide temperature range from 8 to 500 K. Especially above 270 K, $A(T)$ becomes important to describe the non-Gaussian q-behavior.

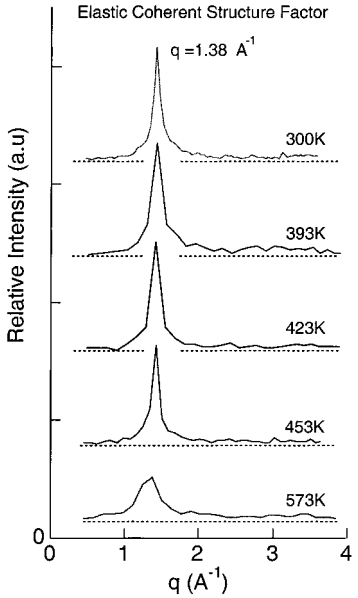

Figure 5. Elastic coherent structure factors for $q_\perp$ at 300, 393, 423, 453, and 573 K, decomposed by neutron polarization analysis. In a temperature region up to 453 K, the intense (110) diffraction at $q = 1.38$ Å^{-1} is stable, while in a nematic phase at 573 K, it becomes broader.

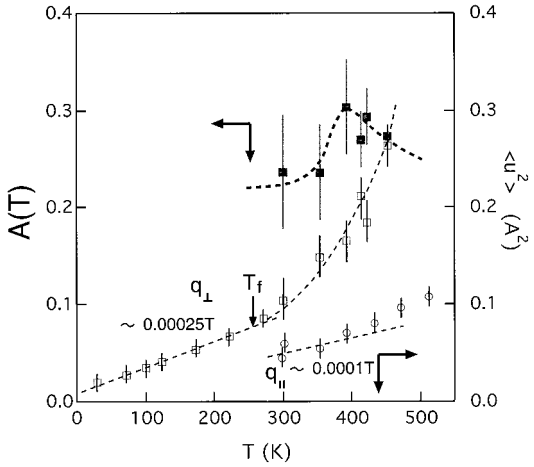

Figure 6. Mean-square displacement $\langle u^2 \rangle$ and non-Gaussian parameter $A(T)$ estimated from asymptotic q-behaviors of the elastic incoherent scattering. Above T_f (≅270 K), $\langle u^2 \rangle$ for $q_\perp$ increases anharmonically, deviating from the harmonic increase of $\langle u^2 \rangle \sim 0.00025T$ below T_f. $\langle u^2 \rangle$ for $q_{||}$ increases harmonically following $\langle u^2 \rangle \sim 0.0001T$. Above T_f, $A(T)$ becomes important for $q_\perp$, exhibiting a maximum value of $A(T) = 0.31$ at 393 K.

Although in the high-temperature region up to 500 K the asymptotic q-behavior is attributed not only to the vibrational motion but also to the relaxation, we employ the Debye−Waller factor of eqs 4 and 5 in order to estimate the apparent mean-square displacement $\langle u^2 \rangle$. Figure 6 shows $\langle u^2 \rangle$ and $A(T)$ obtained for both $q_\perp$ and $q_{||}$. In the temperature region above 270 K (=T_f), $\langle u^2 \rangle$ for $q_\perp$ starts to increase anharmonically, while below 270 K, $\langle u^2 \rangle$ for $q_\perp$ increases linearly following $\langle u^2 \rangle \sim 0.00025T +$ const. Above T_f, we estimate $A(T)$ for $q_\perp$ from the non-Gaussian q-behavior, whose maximum value of $A(T)$ is about 0.36 at around T_g. On the other hand, $\langle u^2 \rangle$ for $q_{||}$ increases linearly, obeying $\langle u^2 \rangle \sim 0.0001T +$ const, even above T_f where the anharmonic increase appears for $q_\perp$. We stress that T_f is about 110 K smaller than T_g. The anharmonic increase of $\langle u^2 \rangle$ at

T_f is an analogous behavior with the fragile or intermediate glass forming materials.[6−11] Furthermore, our results are unique to show the anisotropic $\langle u^2 \rangle$ and $A(T)$, observed in a direction perpendicular to the rigid chain orientation. This anisotrpic anharmonicity would relate to a local molecular structure and its motion, i.e., the torsional or rotational degree of freedom for aromatic rings.

V. Discussion

1. Microcrystal Dispersed in Anisotropic Glassy Matrix. To describe the interchain order below T_m, we stress the two experimental results in the references. The first one is the calorimetric study finding the small difference of the enthalpy ($\Delta H \sim 4-5$ kJ/mol) or the entropy ($\Delta S \sim 6-7$ kJ/(mol K)) at T_m.[29] This result directly indicates that the difference of interchain order between nematic and solid phases is negligibly small. The second one is the WAXS study showing that at 505 K the slow ordering process takes the order of 10^4 min to achieve the orthorhombic segmental packing with the crystallinity of 40%, while the fast process takes the order of a minute to form the low-ordered pseudohexagonal lattice.[24] It is reported in ref 24 that as the crystalline ordering proceeds by the slow process, the (210) reflection grows up in the WAXS profile. The slow process would correspond to the searching process of NPL[37,38] or the conformationally changing process of PCL.[39] We prepared our sample specimen by quenching from above T_m into water. The quenching process was rapid enough to avoid the slow process. Therefore, we can expect that our specimen remains in a glassy state where the microcrystals are dispersed in a huge matrix of glass. On the other hand, the temperature region between 500 K and T_m is very complicated because the interchain order changes dramatically during the slow process. It should be stressed that the recent studies on this material focus on the slow process (see refs 18−39). In this paper, we skip a discussion of segmental motions in the temperature region between 500 K and T_m and focus on the two regions: (i) below 500 K and (ii) above T_m.

2. Non-Gaussianity Observed from T_f to above T_g. We observed the anharmonic increases of $\langle u^2 \rangle$ and the non-Gaussian q-behavior in the temperature region from T_f to above T_g. To examine these results, let us denote general results observed in this temperature region for isotropic polymer glasses. The "time of flight" measurements (TOF) on the polymer glasses elucidated the dynamical crossover of the self-correlation function from the exponential decay at shorter time ($t < t_c \cong 2$ ps) to the stretched-exponential decay at longer time ($t > t_c$).[15,16] The intermediate incoherent scattering function $S(q,t)$, obtained by the Fourier transform of TOF spectra in a energy domain, decays by two steps up to the time of 10^{-10} s. It is suggested that the initial exponential decay of $t < t_c$ is due to the uncorrelated segmental motion in a cage, while the second stretched-exponential decay of $t > t_c$ is due to the cooperative segmental motion. Simultaneously, the second decay is a counterpart of the anharmonic increase of $\langle u^2 \rangle$. The dynamical crossover was discussed qualitatively in terms of a Smoluchowski memory function (see eq 2 in ref 17). In the time domain of $t < t_c$, the memory function $H(q,t)$ might be negligible so that we obtain a simple exponential formalism as a initial decay. In the time domain of $t > t_c$, the memory function starts to contribute on the decay including the cage effect. Along a similar discussion, on the basis of the generalized hydrodynamics theory, MCT has studied the kinetic description of glassy dynamics from a side of the liquid state. The idealized version of MCT predicts the dynamical quantities, e.g., viscosity, diverges at T_c ($\cong 1.2T_g$).[12] On the other hand, the extensive experiments have not observed the dynamical divergence at T_c even for the most fragile glass of *o*-terphenyl.[5] To bury a gap between them, it has been proposed that the energy landscape scenario and activated dynamical process should be taken into account for theoretical treatments as the temperature decreases closer to T_g.[47] Especially for the glassy polymers, the careful investigations indicate the relationship between the anharmonic increase of $\langle u^2 \rangle$ and the carbon−carbon (C−C) torsional motion.[17] It is reported that the temperature T_f is proportional to the activation energy for the C−C torsion. Thus, for glassy polymers, the scenario should consider the torsional or rotational degree of freedom about the C−C bond as an activated process.

Our results shown in this paper coincide with these general observations in the following points. The anharmonic increases of $\langle u^2 \rangle$ for $q_\perp$ is analogous to the universal appearance of the fast β picosecond motion for the fragile or intermediate glass below T_g.[6−11] The onset temperature T_f is about 110 K lower than T_g, which is very close to that of polystyrene[9,10] or polycarbonate.[14] Furthermore, the relation between the anharmonic increase of $\langle u^2 \rangle$ and the C−C torsional motion coincides with our observations, i.e., anisotropically anharmonic increase of $\langle u^2 \rangle$.

On the basis of these observations, we describe our system as follows. In the low-temperature region far below T_f, the aromatic ring is trapped in a bottom of the cage. In this regime, the bottom shape determines the aromatic ring's motion. The harmonic increase of $\langle u^2 \rangle$ with temperature below T_f strongly supports the harmonic vibration and the bottom shape of a quadratic form. In ref 48, we observed the non-Gaussian q-behavior of the elastic incoherent scattering, focusing on the outside of the low-energy region with incident neutron of $\lambda = 1.54$ Å ($\Delta E = 2.8$ meV). In the low-temperature region below T_f, we determined $A(T)$ ($\cong 0.25$) for $q_\perp$, employing eqs 4 and 5. The non-Gaussianity below T_f seems to be general observations at least for the glassy or partially crystallized polymers.[49,50] In ref 51, the origin of $A(T)$ was discussed from a static point of view, where we utilize the word "static" as a meaning "infinite-time living". In general, the non-Gaussian q-behavior originates from (i) the anharmonic vibration, (ii) the distribution of harmonic vibration, and (iii) the local anisotropy of motion.[51] We stress that the non-Gaussian parameter $A(T)$ observed in ref 48 is positive for all temperatures, which supports the scenario of the static distribution of harmonic vibrations.

In the temperature region from T_f ($= T_g - 110$ K) to above T_g, the aromatic ring starts to move with excess $\langle u^2 \rangle$ for the direction along $q_\perp$. This excess $\langle u^2 \rangle$ increases anharmonically with temperature. In this regime, the recent MD study has revealed that the energy landscape itself changes dramatically and the cage becomes loose.[52] The torsional motion in the loose cage would give the anharmonic increase of $\langle u^2 \rangle$. We estimated the non-Gaussian parameter of the order of 0.3 at around T_g. If this non-Gaussianity is attributed to the static heterogeneity of vibrational (or torsional) motion, this scenario

matches the stretched exponential relaxation reported by the TOF measurements.[15−17] The positive $A(T)$, determined in Figure 6, would be attributed to the static heterogeneity for torsional motions in the loose cage. We propose that the energy landscape becomes more anisotropic in this region, reflecting the anisotropic $\langle u^2 \rangle$ and $A(T)$.

We should make a comment on another interpretation of the non-Gaussian q-behavior of the elastic incoherent scattering, e.g., EISF for two sites jump motion between cages. Richter et al. reported that the two sites jump motion with a jump distance $d = 0.65-0.7$ Å well reproduces the elastic and QEL incoherent scattering observed for polyisobutylene in the β regime.[53] We performed the data analysis for the elastic incoherent scattering for $q_\perp$ from 300 to 453 K, following the scenario of the two sites jump. If d is monodispersed and there is no correlation between the vibrational motion at the bottom of cages and the jump motion, we obtain a scattering function for the two sites jump motion for an isotropic system:

$$S_{\mathrm{inc}}(q,\omega=0) \sim \exp(-\langle u^2 \rangle q^2)\{^1/_2[1 + \sin(qd)/(qd)]\} \quad (10)$$

For this analysis, we determined $\langle u^2 \rangle$ from 300 to 453 K to extrapolate the harmonic relation for $q_\perp$ of $\langle u^2 \rangle \sim 0.00025T +$ const observed below 300 K. As a result of curve fittings with eq 10, we obtained the jump distance of $d = 0.65-1.0$ Å for temperatures from 300 to 453 K. Especially, the jump distance of $d = 1.0$ Å estimated at 453 K is close to a size of the benzoic ring, suggesting that above 453 K the aromatic rings would start a flip-flop motion. However, the two sites jump motion of eq 10 is based on an ideal picture of the monodispersed tight cage at around T_g, where there coexists the harmonic vibration in the bottom of a quadratic form and jumping between two basins. As indicated in ref 52, the static heterogeneity for a distance between basins and its energy barrier is a key to describe the energy landscape. Thus, we would need to modify eq 10 to consider the static distribution of both the jump distance and the jump rate. On the other hand, our analysis, performed in section IV.3, is based on the picture of loosening a cage with temperature and the static heterogeneity of torsion in a loose cage.

Even above T_g, the estimated $A(T)$ seems to be temperature-independent within the error bars. From a kinetic point of view, we would propose the attractive possibility of the temperature-independent $A(T)$. As investigated by Rahman, the non-Gaussian parameter is intrinsically time-dependent $A(t)$.[44] The recent MD study for glass forming particles identified the kinetic heterogeneity through the time-dependent non-Gaussian parameter.[54,55] The weakly bonded mobile domains (or cooperatively rearranging regions) appear on time scales shorter than τ_α (or in β regime) (see Figure 7). However, these regions disappear and become homogeneous on time scales longer than τ_α .[55] The spatial average of kinetic heterogeneity leads to the positive non-Gaussian parameter as a function of time. On the other hand, the elastic scattering experiment provides a snapshot picture taken with a shutter speed of $h/\Delta E$. Figure 7 shows our experimental situation schematically. According to our experimental condition, the value of $h/\Delta E$ is the order of 5×10^{-12} s, which is identical with the β regime. If our elastic window matches properly, we would observe the time- and temperature-dependent $A(t)$, which originates from the intrinsic kinetic property for glasses. This is our future work.

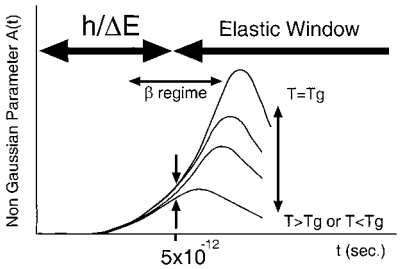

Figure 7. Schematic diagram for the time-dependent non-Gaussian parameter $A(t)$ observed through an elastic window having an energy resolution ΔE.

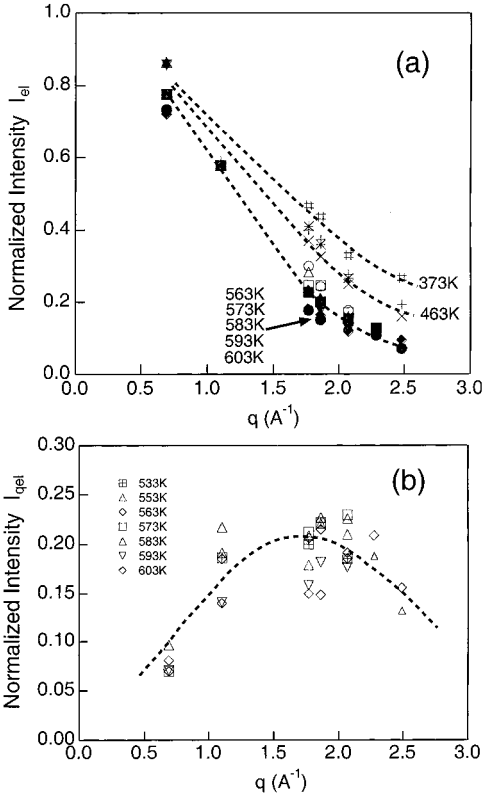

Figure 8. Normalized intensity of (a) elastic component I_{el} and (b) quasi-elastic component I_{qel}, decomposed from constant q-scan profiles. The broken lines are guides for the eye.

V.3. Free Rotational Motion above T_m. In ref 46, we have discussed the rotational motion of aromatic rings in a nematic phase above T_m, observed through the QEL neutron scattering in the energy region lower than 2 meV. The q dependence of hwhh of QEL spectra was well reproduced by the free rotational model (see section III). As shown in Figure 2b, we decompose the constant q-profiles into the elastic and QEL components to obtain the normalized intensity I_{ela} and I_{qel}. The q positions for the constant q-scan were chosen to avoid the coherent contribution. Parts a and b of Figure 8 show the normalized intensity of elastic and QEL components I_{ela} and I_{qel}, respectively. As the temperature increases, I_{ela} decreases more rapidly with q. Above T_m, I_{ela} shows the minimum value at around $q = 2.5$ Å^{-1}. On the other hand, the q-behavior of I_{qel} is characteristic of exhibiting a broad maximum at around 1.5−2.0 Å^{-1}.

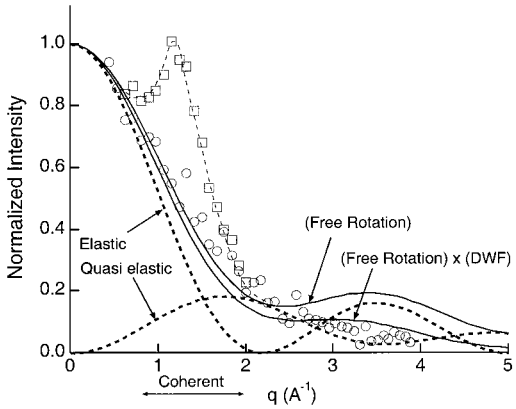

Figure 9. Model analysis of elastic scattering profiles above T_m, based on the free rotational model. The open squares and circles indicate the elastic coherent and elastic incoherent scattering components, decomposed by neutron polarization analysis. The thick broken lines are elastic and quasi-elastic contributions, calculated with $r \sin \phi = 1.1$ and $\varphi = 0.5$. The solid lines indicate a total contribution from elastic and quasi-elastic components, where the steeper profile takes into account the Debye−Waller factor contribution.

As related with these observations, we examine the elastic incoherent scattering profile above T_m obtained by neutron polarization analysis. Figure 9 shows the decomposed elastic scattering profiles. The open circles show the incoherent scattering components at 603 K ($=T_g + 220$ K). We plot the total elastic scattering (open squares). The thick broken lines indicate the elastic and QEL components calculated by the free rotation model with the apparent radius $r \sin \phi = 1.1$. The solid lines indicate the total contribution of both elastic and QEL components with $\varphi = 0.5$ in eq 3. The solid line, which decreases steeper with q, takes into account the harmonic DWF, in which $\langle u^2 \rangle$ is extrapolated with the linear relationship for $q_{\parallel}$, $\langle u^2 \rangle \sim 0.0001T +$ const. The calculated curve describes well the measured incoherent scattering profile. Simultaneously, the calculated elastic and quasi-elastic lines reproduces well the q-behavior of I_{ela} and I_{qel} in Figure 8. The q-behavior of hwhh of QEL spectra, discussed in ref 46, was reproduced with $r \sin \phi = 1.6$. For a better interpretation, it is crucial to consider the distribution of $r \sin \phi$ around $r \sin \phi = 1.1-1.6$, which would be attributed to the heterogeneity of $r \sin \phi$ or the orientational distribution of the rigid chain in a nematic phase.

Although our discussion is limited to a qualitative level, our observation seems to support the free rotation of the aromatic rings about the rigid chain backbone. In this temperature region, the memory function might become negligible enough to rotate obeying the Fickian diffusion. The individual aromatic rings suffers from a mean field friction ζ ($\sim 1/D_r$), which is determined mainly by the intrachain interaction. Windle et al. investigated an isolated glassy copolyester by the quantum mechanical computation.[56] It is reported that as a result of competing factors of the steric repulsion and the resonance stabilization, the so-called T-dihedral angles of phenyl benzoate rotate easily, having the lower energy barrier and its smaller angular dependence. This calculation strongly supports our interpretation above T_m. As the temperature decreases, on the other hand, the interchain interaction becomes crucial to determining the segmental motion.

VI. Conclusions

We investigated the segmental motion of supercooled random copolyester through the elastic window of neutron scattering. We applied neutron polarization analysis to obtain the coherent and incoherent scattering components. A careful discussion of the non-Gaussianity of the elastic incoherent scattering or EISF elucidates the following points. At the temperature T_f ($\cong$ 270 K), which is about 110 K smaller than T_g, we observed the anharmonic increase of $\langle u^2 \rangle$ only for a direction perpendicular to the rigid chain direction ($q_{\perp}$). Simultaneously, the non-Gaussian q-behavior of the elastic incoherent scattering becomes obvious for $q_{\perp}$. These observations coincide with the recent reports on the correlation between the carbon−carbon (C−C) torsional energy and the anharmonic increase of $\langle u^2 \rangle$. The crossover is attributed to a change from a tight cage to a loose cage for the segmental packing. In a nematic phase above T_m, the elastic incoherent scattering profiles were well reproduced by EISF for the Fickian free rotational model. This model describes well the QEL scattering in terms of its q dependence of width and intensity.

Acknowledgment. We thank T. Shiwaku of Polyplastic Co. Ltd. for supplying a sample specimen. We are also grateful to T. Kanaya of Kyoto University for helpful discussions.

References and Notes

(1) Richter, D.; Frick, B. *Science* **1995**, *267*, 1939.
(2) Moon, R. M.; Riste, T.; Koehler, W. C. *Phys. Rev.* **1969**, *181*, 920.
(3) Williams, W. G. *Polarized Neutrons;* Oxford Series on Neutron Scattering in Condensed Matter No.1; Oxford University Press: New York. Squires, G. L. *Introduction to The Theory of Thermal Neutron Scattering*; Dover Publications: New York.
(4) Biswas, A. *J. Polym. Sci., Polym. Phys. Ed.* **1992**, *30*, 1375.
(5) Angell, C. A. *Science* **1995**, *267*, 1924. Angell, C. A. *J. Phys. Chem. Solids* **1988**, *49*, 863. Angell, C. A. *J. Non-Cryst. Solids* **1988**, *102*, 204.
(6) Debus, O.; Zimmermann, H.; Bartsch, E.; Fujara, F.; Kiebel, M.; Petry, W.; Sillescu, H. *Chem. Phys. Lett.* **1991**, *180*, 271.
(7) Frick, B.; Richter, D.; Zorn, R.; Fetters, L. J. *J. Non-Cryst. Solids* **1994**, *172/174*, 272.
(8) Kanaya, T.; Kaji, K.; Inoue, K. *Macromolecules* **1991**, *24*, 1826. Kanaya, T.; Kawaguchi, T.; Kaji, K. *J. Chem. Phys.* **1993**, *98*, 8262.
(9) Kanaya, T.; Kawaguchi, T.; Kaji, K. *J. Chem. Phys.* **1995**, *104*, 3841.
(10) Frick, B.; Buchenau, U.; Richter. D. *Colloid Polym. Sci.* **1995**, *273*, 413−420.
(11) Kanaya, T.; Kawaguchi, T.; Kaji, K. *J. Chem. Phys.* **1996**, *105*, 4342.
(12) Götze, W. In *Liquids, Freezing and the Glass Transition*; Hansen, J. P., Leuesque, D., Zinn-Justin, J., Eds.; North-Holland: Amsterdam, 1989. Götze, W.; Sjögren, L. *Rep. Prog. Phys.* **1992**, *55*, 241.
(13) Buchenau, U.; Zorn, R. *Europhys. Lett.* **1992**, *18*, 523. Buchenau, U. *Philos. Mag.* **1992**, *65*, 303.
(14) Buchenau, U.; Schönfeld, C.; Richter, D.; Kanaya, T.; Kaji, K.; Wehrmann, R. *Phys. Rev. Lett.* **1994**, *73*, 2344.
(15) Colmenero, J.; Arbe, A.; Alegria, A. *Phys. Rev. Lett.* **1993**, *71*, 2603. Colmenero, J.; Arbe, A.; Alegria, A. *J. Non-Cryst. Solids* **1994**, *192−174*, 126. Colmenero, J.; Arbe, A.; Coddens, G.; Frick, B.; Mijangos, C.; Reinecke, H. *Phys. Rev. Lett.* **1997**, *78*, 1928.
(16) Zorn, R.; Arbe, A.; Colmenero, J.; Frick. B.; Richter, D.; Buchenau, U. *Phys. Rev. E* **1995**, 52, 781.
(17) Colmenero, J.; Arbe, A. *Phys. Rev. B* **1998**, *57*, 13508.
(18) Gutierrez, G. A.; Chivers, R. A.; Blackwell, J.; Stamatoff, J. B.; Yoon, H. *Polymer* **1983**, *24*, 937.
(19) Chivers, R. A.; Blackwell, J.; Gutierrez, G. A. *Polymer* **1984**, *24*, 435.

(20) Blackwell, J.; Gutierrez, G. A.; Chivers, R. A. *Macromolecules* **1984**, *17*, 1219.
(21) Blackwell, J.; Gutierrez, G. A.; Chivers, R. A.; Ruland, W. J. *J. Polym. Sci., Polym. Phys. Ed.* **1984**, *22*, 1343.
(22) Mitchell, G. R.; Windle, A. H. *Colloid Polym. Sci.* **1985**, *263*, 230.
(23) Windle, A. H.; Viney, C.; Golombok, R.; Donald, A. M.; Mitchell, G. R. *Faraday Discuss. Chem Soc.* **1985**, *79*, 55.
(24) Cheng, S. Z. D.; Janimak, J. J.; Zhang, A.; Zhou, Z. *Macromolecules* **1989**, *22*, 4240.
(25) Kaito, A.; Kyotani, M.; Nakayama, K. *Macromolecules* **1990**, *23*, 1035.
(26) Flores, A.; Ania, F.; Calleja, F. J. B.; Ward, I. M. *Polymer* **1993**, *34*, 2915.
(27) Wilson, D. J.; Vonk, C. G.; Windle, A. H. *Polymer* **1993**, *34*, 227.
(28) Hanna, S.; Lemmon, T. J.; Spontak, R. J.; Windle, A. H. *Polymer* **1992**, *33*, 3.
(29) Wunderlich, B.; Grebowicz, J. *Adv. Polym. Sci.* **1984**, *60/61*, 1.
(30) Cheng, S. Z. D. *Macromolecules* **1988**, *21*, 2475.
(31) Yonetake, K.; Sagiya, T.; Koyama, K.; Masuko, T. *Macromolecules* **1992**, *25*, 1009.
(32) Clements, J.; Humphreys, J.; Ward, I. M. *J. Polym. Sci. B, Polym. Phys.* **1986**, *24*, 2293.
(33) Allen, R. A.; Ward, I. M. *Polymer* **1991**, *32*, 202.
(34) Kalika, D. S.; Yoon, D. Y. *Macromolecules* **1991**, *24*, 3404.
(35) Blundell, D. J.; Buckingham, K. A. *Polymer* **1985**, *26*, 1623.
(36) Troughton, M. J.; Davies, G. R.; Ward, I. M. *Polymer* **1989**, *30*, 58.
(37) Hanna, S.; Windle, A. H. *Polymer* **1988**, *29*, 207.
(38) Hanna, S.; Romo-Uribe, A.; Windle, A. H. *Nature* **1993**, *366*, 546.
(39) Hofmann, D.; Schneider, A. I.; Blackwell, J. *Polymer* **1994**, *35*, 5603.
(40) Koizumi, S.; et al., unpublished.
(41) Dore, J. C.; Clarke, J. H.; Wenzel, J. T. *Nucl. Instrum. Methods* **1976**, *138*, 317.
(42) Bee, M. *Quasielastic Neutron Scattering: Principles and Applications in Solid State Chemistry, Biology and Materials Science*; Adam Hilger: Bristol, U.K., 1988.
(43) Lovsey, S. W. *Theory of Neutron Scattering from Condensed Matter*; Oxford Science Publications: Oxford, 1984.
(44) Rahman, A. *Phys. Rev.* **1964**, *136*, A405.
(45) Dianoux, A. J.; Volino, F.; Hervet, H. *Mol. Phys.* **1975**, *30*, 1181. Bee, M.; Dianoux, A. J.; Volino, F. *Mol. Phys.* **1984,** *51*, 221.
(46) Koizumi, S. *J. Chem. Phys.* **1997**, *107*, 603.
(47) Angell, C. A. *J. Phys. Chem. Solids* **1988**, *49*, 863.
(48) Koizumi, S., manuscript in preparation.
(49) Kanaya, T.; Tukushi, I.; Kaji, K.; Gabrys, B.; Bennington, S. M. *J. Non-Cryst. Solids* **1998**, *212−218*, 235.
(50) Kanaya, T.; Buchenau, U.; Koizumi, S.; Tukushi, I.; Kaji, K., manuscript in preparation.
(51) Zorn, R. *Phys. Rev. B* **1997**, *55*, 6249.
(52) Stillinger, F. H. *Science* **1995**, *267*, 1935. Sastry, S.; Debenedett, P. G.; Stillinger, F. H. *Nature* **1998**, *393*, 554.
(53) Richter, D.; Arbe, A.; Colmenero, J.; Monkenbusch, M.; Farago, B.; Faust, R. *Macromolecules* **1998**, *31*, 1133.
(54) Kob, W.; Dotani, C.; Plimpton, S. J.; Poole, P. H.; Glotzer, S. C. *Phys. Rev. Lett.* **1997**, *79*, 2827. Dotani, C.; Douglas, J. F.; Kob, W.; Plimpton, S. J.; Poole, P. H.; Glotzer, S. C. *Phys. Rev. Lett.* **1998**, *80*, 2338.
(55) Yamamoto, R.; Onuki, A. *Phys. Rev. E* **1998**, *58*, 3515.
(56) Coulter, P.; Windle, A. H. *Macromolecules* **1989**, *22*, 1129.

MA981876H